Active MMIC Circulator Performance in a Phased-Array-Like Environment

Laila Marzall[1], Shane Verploegh[1], Tommaso Cappello[1], Michael Roberg[2], Zoya Popović[1]

[1] University of Colorado Boulder, USA

[2] Qorvo, Richardson, USA

{[1]Laila.Marzall, [1]Shane.Verploegh, [1]Tommaso.Cappello, [1]Zoya.Popovic }@colorado.edu

Abstract — This paper presents an analysis of a 8-12 GHz active $0.25\,\mu$m GaAs pHEMT MMIC circulator intended for integration into a phased array. The architecture is based on a closed-loop connection of three asymmetric -5.6-dB Lange couplers and resistive-feedback gain-matched amplifiers. The nominal simulated performance shows an isolation of 20 dB over a 40% bandwidth, with a return loss of better than 10 dB and an insertion gain of 2.4 dB across the band. The degradation in circuit performance is analyzed as a function of variations in port impedance. A loop-gain analysis demonstrates the circuit stability for port impedances in the VSWR = 2 circle, simulating coupling in a phased array. We show in simulation and measurements that the bandwidth, match on all ports and insertion gain are not sensitive and agree with simulations. However, the isolation degrades from 20 dB when the port impedances change within a VSWR=1.1 circle. Additionally, we show that the deviation of the coupler design from the nominal case affects the isolation. The statistical analysis gives insight into design criteria of this type of circulator for insertion into phased array.

Keywords — active circulators, Lange couplers, MMIC, electronically steered phased arrays, T/R modules, RF front-ends.

I. INTRODUCTION

Non-reciprocal behavior of transistors can be used to achieve circulation and was first presented in 1965 [1]. In transistor-based devices, the distinction is made between active 3-way circulators with full rotational symmetry (as in a ferrite device), and quasi-circulators that have isolation between two of the ports but do not have full circulation. Different topologies of active MMIC circulators and quasi-circulators with the use of quadrature hybrids have been demonstrated in [2], [3] and [4]. Noise performance and power limitation analysis, as well as design techniques for simultaneous optimization are described in [5], [6], and [7]. In addition, integration with antennas is discussed in [8], [9].

Here we present a 8-12 GHz GaAs MMIC active circulator with gain. The architecture is based on a closed-loop connection of three broadband couplers and gain-matched amplifiers, Fig.1a. A resistive-feedback unit amplifier is implemented in a 0.25 μm GaAs pHEMT monolithic microwave integrated circuit (MMIC) process with asymmetric -5.6 - dB Lange couplers. The nominal simulated performance shows an isolation of 20 dB over a 40% bandwidth, with a return loss of better than 10 dB and an insertion gain of 2.4 dB across the band. The 2.5 mm × 2.5 mm chip shown in Fig.1b is analyzed in terms of behavior when integrated in a phased
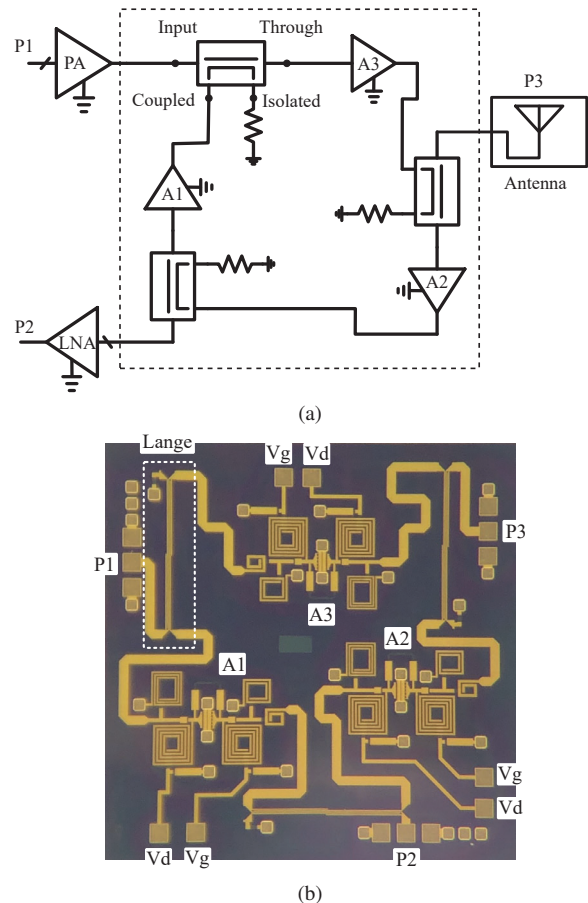

(a)

(b)

Fig. 1. (a) Block diagram of the active circulator and possible use in a transmission-reception (T/R) module. The transistors give isolation and gain, while the asymmetric couplers improve stability and bandwidth. (b) Layout and photograph of a 2.5 mm × 2.5 mm GaAs MMIC X-band implementation.

array environment, where the port impedances vary and where process variations impact device performance.

II. CIRCUIT TOPOLOGY AND DESIGN

The three-port active circulator topology is intended to be inserted in a phased array front end as shown in Fig.1a, where $|S_{31}|$ and $|S_{23}| \approx 1$, $|S_{13}|$, $|S_{32}|$ and $|S_{21}| \approx 0$, with all three ports matched. Such behavior is accomplished by connecting three single-stage unconditionally-stable, gain-matched, identical amplifiers with three 4-port couplers. The *through* ports are connected to
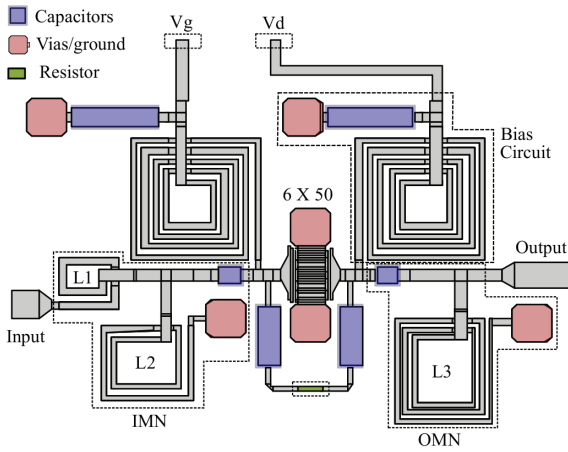
12 – 14 January 2021, Utrecht, The Netherlands

Fig. 2. Unit amplifier layout, showing the $200\,\Omega$ feedback resistor and $0.9\,\text{pF}$ blocking capacitors. The gate and drain bias circuits use $4\,\text{pF}$ bypass capacitors and $3.9\,\text{nH}$ spiral inductors. The maximum dimensions are $1050\,\mu\text{m}\times700\,\mu\text{m}$. Input and output matching networks are implemented with shunt inductors $L_1 = 0.45\,\text{nH}$ and $L_2 = 0.89\,\text{nH}$, and a series inductor $L_3 = 2.12\,\text{nH}$.

the amplifier inputs, and the *coupled* ports to the outputs. The *isolated* ports are terminated in 50-Ω resistors. During the design process, the Lange coupler length is varied to reach a trade-off between isolation ($|S_{31}|$) and transmission gain ($|S_{21}|$), while ensuring stability. The forward gain of the circulator is proportional to the amplifier gain, reduced by the *coupling* and *through* attenuation of the Lange couplers.

The small-signal gain-matched amplifier is designed around a $6\times50\,\mu\text{m}$ depletion-mode pHEMT biased in class A at $V_D = 5\,\text{V}$ and with $V_G = -0.3\,\text{V}$. The unit amplifier layout is shown in Fig. 2. Line widths greater than $4\,\mu\text{m}$ are used to meet the current handling requirement of $72\,\text{mA}$ with a safety margin. The biasing circuits are implemented with $3.95\,\text{nH}$ spiral inductors, $4\,\text{pF}$ bypass and $0.9\,\text{pF}$ blocking capacitors. To improve stability and increase bandwidth, a $R = 200\,\Omega$ feedback resistor is connected with high-impedance short lines between gate and drain terminals. Input and output matching networks are implemented with shunt inductors $L_1 = 2.1\,\text{nH}$ and $L_2 = 0.89\,\text{nH}$, and a series inductor $L_3 = 0.45\,\text{nH}$.

To understand the impact of the coupler on circulator parameters, consider the sub-circuits in Fig.3(a) and (b). The ideal matched coupler S-parameters can be expressed analytically as:

$$a = \frac{\sqrt{1-c^2}}{\sqrt{1-c^2}\cos\beta l + j\sin\beta l} \qquad (1)$$

$$b = \frac{jc\tan\beta l}{\sqrt{1-c^2} + j\tan\beta l} \qquad (2)$$

where c is the coupling coefficient is a value between 0 and 1, and βl is the electrical length of the coupled-line section. The circulator behavior is affected by both the coupling coefficient and the length of the coupler. Fig.4 shows the simulated S-parameters of a (a) 3-dB and (b) 6-dB coupler for two line lengths: $\lambda/4$ and $\lambda/10$, showing that the circulator gain and isolation are affected by either the coupling coefficient or the length of the line, while the match and bandwidth are
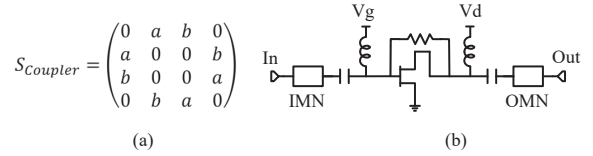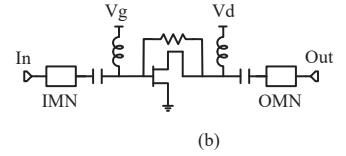
(a)   (b)
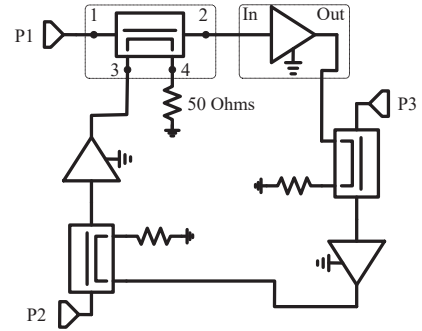
(c)

Fig. 3. Sub-circuits of the active circulator: (a) equation-based model of a 4-port ideal coupler; (b) unit amplifier with resistive feedback; (c) circulator with three sub-circuits (a) and (b) connected into a single 3-port network.
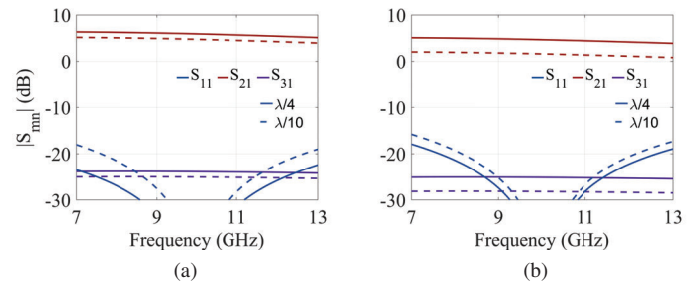

Fig. 4. Simulated S-parameters of the active circulator with the same amplifier, using (a) $C = 3\,\text{dB}$ and (b) $C = 6\,\text{dB}$ couplers for two different coupled-line section lengths: $\lambda/4$ and $\lambda/10$.

not dramatically affected. In particular, the isolation is high because of the ideality of the coupler, and therefore depends on S_{12} of the amplifiers.

With this in mind, we analyze how the Lange coupler S-parameters depend on length and coupling coefficient, illustrated in Fig.5. For a coupler length of 2.5 mm ($\lambda_g/4$ on the MMIC substrate) and with 4 fingers, a parametric simulation is performed with line separations between 2 and 5 μm and shown in Fig.5a. When the coupler length is varied between 2.5 mm and 1 mm ($\lambda_g/10$) and with a line separation of 3 μm, the results are shown in Fig.5b. The implication of this study is that even for couplers with the same coupling coefficient, the isolation can vary depending on length, and will impact circulator isolation and bandwidth. For the final design, we adopt a Lange coupler l=1 mm long with a spacing of 3 μm between each of the 4 lines, resulting in $|S_{21}| \approx -1.4\,\text{dB}$ and $|S_{31}| \approx -5.9\,\text{dB}$, with a match and isolation better than -30 dB over 8-12 GHz after full-wave simulations.

The closed-loop topology from Fig. 1a requires careful stability analysis, because odd-mode oscillations can occur but will not be detected by K-factor analysis. An open-loop gain analysis [10] is performed by extracting the locally linearized,
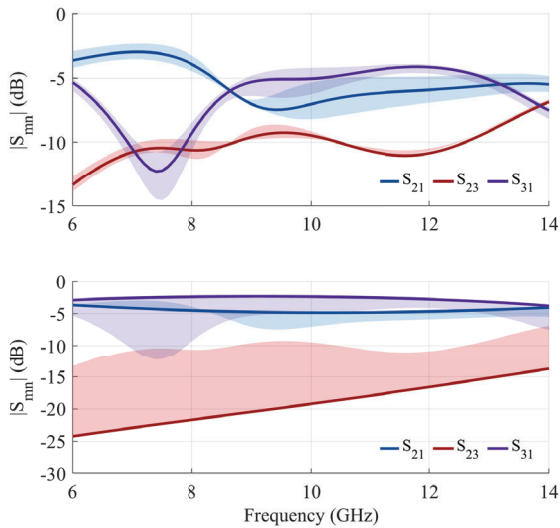
Fig. 5. Lange coupler simulated S-parameter parametric study. (a) The coupler length is 2.5 mm ($\lambda_g/4$) and the line separations varies between 2 and 5μm. (b) The coupler length is varied between 2.5 mm and 1 mm ($\lambda_g/10$) and the line separation kept at 3μm. The nominal case with $l = 2.5$ mm and separation of 3μm is shown in solid line.
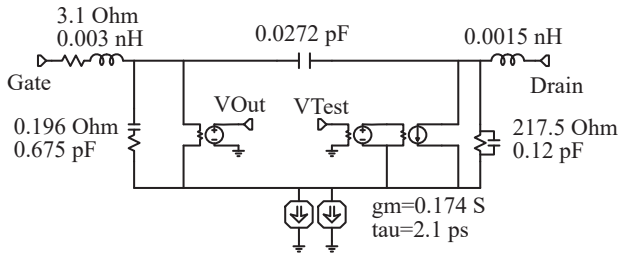

Fig. 6. Small-signal model extracted from transistor foundry nonlinear model and adapted to open-loop stability analysis.

intrinsic small-signal model of the device (Fig. 6) and using it in the EM-simulated circuit in place of the foundry model. The polar plot in Fig. 7 shows the feedback voltage gain for the three devices over frequency and with external port impedances of 50 Ω (solid lines). Stability is ensured when V_{Out}/V_{Test} does not cross the positive horizontal axis for amplitudes larger than unity. In normal operation, a circulator is connected to three different loads (PA, LNA and antenna. In an active electronically-steered phased array, these loads can vary, so it is important to investigate stability under different load impedance variations. The shaded plots in Fig.7 show that the phase margin for this circuit is larger than $30°$ for all loads that fall within the VSWR=2 circle on all three ports, with a uniform statistical distribution of impedance values.

III. MEASUREMENTS AND ANALYSIS

Figure 8 shows the chip mounted in a biasing fixture. the on-chip dc pads are wire-bonded to external bias lines. To avoid low frequency instabilities, single layer and SMD capacitors are connected in shunt to the bias lines. The RF ports are 150 - μm GSG pads. A chip was chosen from a production batch for mounting, and measured using a multiport
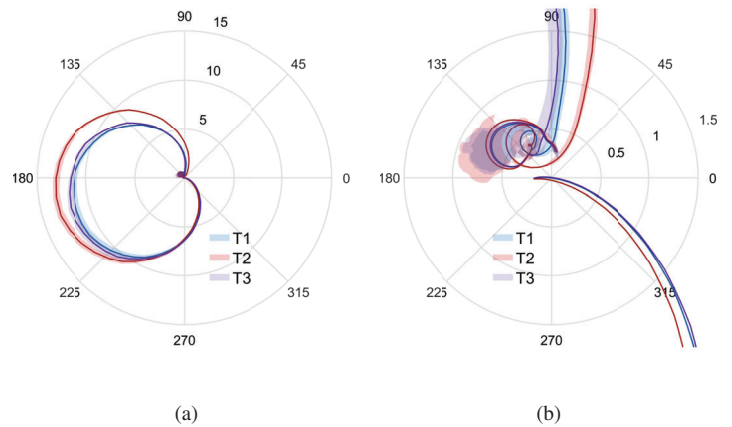

Fig. 7. (a) Simulated loop gain for the three transistors (T1, T2, T3) when ports are terminated with loads within the VSWR=2 circle, from DC to 20 GHz. (b) Detail within magnitude of 1.5.
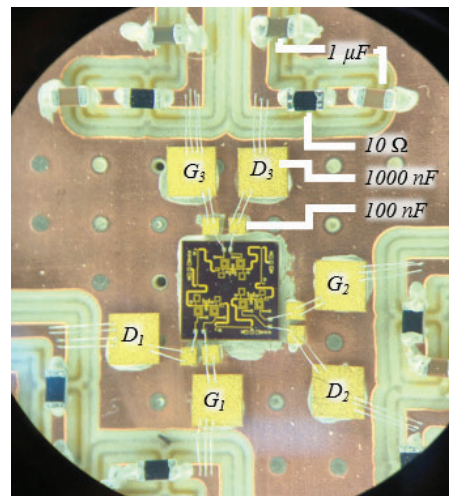

Fig. 8. DC biasing board with chip mounted. Single layer and SMD capacitors are placed in the bias lines, connected with bondwires to on-chip DC pads. The gates bias lines are identified by G1, G2, G3 and and drains D1, D2, D3, respectively. The RF ports are 150-μm GSG probe pads.

PNA with with a 3-port calibration done to the coaxial connector of the probes.

Measurements are compared to simulations in Fig. 9 at nominal bias. The gain (and matching, not shown) agrees well, but the isolation is degraded over the band. To understand this, a statistical analysis is performed with information provided by Qorvo for their process variation, and with additional load mismatch on all three ports inside the VSWR=1.1 circle with a normal distribution of impedances. The results are shown in Fig. 10. Note that this analysis shows a large spread in the three isolation parameters, and that for some values of process parameters and load impedances, the degradation in the measurement is predicted.

IV. CONCLUSION

The design of an active circulator MMIC with gain is presented with a sensitivity analysis emulating the application
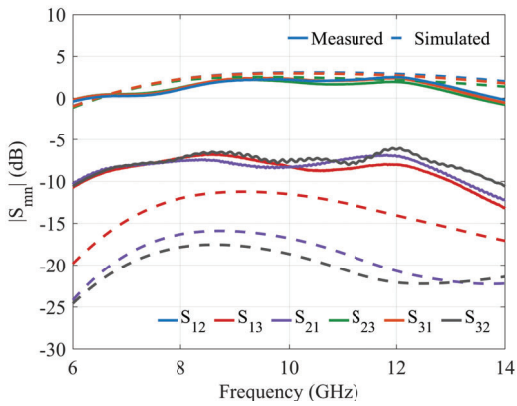
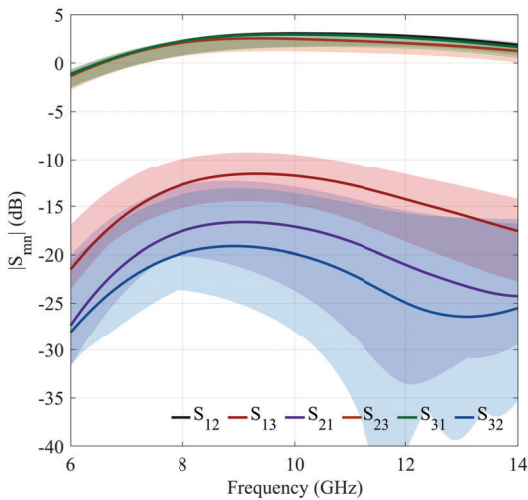Fig. 9. Measured and simulated S-parameters of the circuit from Fig.8.

Fig. 10. Statistical analysis of gain and isolation on all three ports with process variation and loads within a VSWR=1.1 circle.

in a phased-array system. Simulated S-parameters show a circulator behavior with 2.4 dB forward gain, over 20 dB isolation and better than 14 dB match from 8 to 12 GHz, which compares well to previously demonstrated devices summarized in Table1. Measurements show discrepancy in isolation levels when compared to simulations, motivating the statistical analysis, which points to relevant parameters that should be taken into account, and a systematic approach to design of active circulators.

ACKNOWLEDGMENT

REFERENCES

[1] S. Tanaka, N. Shimomura, and K. Ohtake, "Active circulators amp;—the realization of circulators using transistors," *Proceedings of the IEEE*, vol. 53, no. 3, pp. 260–267, Mar. 1965.

Table 1. Comparison of Active MMIC Circulator Performance [4]

Ref	BW (GHz)	$|S_{31}|$ (dB)	$|S_{21}|$ (dB)	$|S_{11}|$ (dB)	Technology	Size (mm²)
[3]	10.2-12.6	-30	+1.5	<-17	0.25 um pHEMT	25
[11]	1.5 - 2.7	-26	+2	-10	CMOS	0.25
[12]	1.5 - 9.6	-18	-6	<-10	0.18 um CMOS	0.41
[6]	3.8 - 4.2	-22	+7.6	-15	MESFET	5
[13]	35 - 40	-30	-5	-15	0.25 um InP-HFET	3.32
[14]	6-18	-12	-2	-12	0.5 um GaAs MESFET	3.10
[15]	0.1-10	-16	-7	-13	0.5 um GaAs FET	0.9

[2] S. M. Hanna and J. Keane, "Analysis and applications of quadrature hybrids as rf circulators," in *Proceedings of International Conference on Particle Accelerators*, 1993, pp. 1118–1120 vol.2.

[3] S. Cheung, T. Halloran, W. Weedon, and C. Caldwell, "Active quasi-circulators using quadrature hybrids for simultaneous transmit and receive," in *2009 IEEE MTT-S International Microwave Symposium Digest*, 2009, pp. 381–384.

[4] S. K. Cheung, T. P. Halloran, W. H. Weedon, and C. P. Caldwell, "Mmic-based quadrature hybrid quasi-circulators for simultaneous transmit and receive," *IEEE Transactions on Microwave Theory and Techniques*, vol. 58, no. 3, pp. 489–497, 2010.

[5] S. Furukawa and S. Horiguchi, "The noise performance of the active circulator," *Proceedings of the IEEE*, vol. 55, no. 11, pp. 2048–2050, Nov. 1967.

[6] A. Gasmi, B. Huyart, E. Bergeault, and L. Jallet, "Noise and power optimization of a mmic quasi-circulator," *IEEE transactions on microwave theory and techniques*, vol. 45, no. 9, pp. 1572–1577, 1997.

[7] G. Carchon and B. Nanwelaers, "Power and noise limitations of active circulators," *IEEE Transactions on Microwave Theory and Techniques*, vol. 48, no. 2, pp. 316–319, Feb. 2000.

[8] M. J. Cryan and P. S. Hall, "An integrated active circulator antenna," *IEEE Microwave and Guided Wave Letters*, vol. 7, no. 7, pp. 190–191, Jul. 1997.

[9] A. Ohlsson, V. Gonzalez-Posadas, and D. Segovia-Vargas, "Active integrated circulating antenna based on non-reciprocal active phase shifters," in *Proc. Second European Conf. Antennas and Propagation EuCAP 2007*, Nov. 2007, pp. 1–5.

[10] M. Roberg, "Loop gain envelope evaluation for rapid mmic amplifier stability analysis," in *2019 IEEE Texas Symposium on Wireless and Microwave Circuits and Systems (WMCS)*. IEEE, 2019, pp. 1–4.

[11] Y. Zheng and C. E. Saavedra, "Active quasi-circulator mmic using otas," *IEEE Microwave and Wireless Components Letters*, vol. 19, no. 4, pp. 218–220, 2009.

[12] S. Shin, J. Huang, K. Lin, and H. Wang, "A 1.5–9.6 ghz monolithic active quasi-circulator in 0.18um cmos technology," *IEEE Microwave and Wireless Components Letters*, vol. 18, no. 12, pp. 797–799, 2008.

[13] M. Berg, T. Hackbarth, B. Maile, S. Kosslowski, J. Dickmann, D. Kother, B. Hopf, and H. Hartnagel, "Active circulator mmic in cpw technology using quarter micron inalas/ingaas/inp hfets," in *Proceedings of 8th International Conference on Indium Phosphide and Related Materials*. IEEE, 1996, pp. 68–71.

[14] P. Katzin, Y. Ayasli, L. D. Reynolds Jr, and B. E. Bedard, "6 to 18 ghz mmic circulators," vol. 35, 01 1992.

[15] S. Hara, T. Tokumitsu, and M. Aikawa, "Novel unilateral circuits for mmic circulators," *IEEE Transactions on Microwave Theory and Techniques*, vol. 38, no. 10, pp. 1399–1406, 1990.